Identification of K^+-mesons from subthreshold pA collisions with ANKE at COSY-Jülich

M. Büscher [a], H. Junghans [a], V. Koptev [b], M. Nekipelov [b], K. Sistemich [a], H. Ströher [a], S. Barsov [b], G. Borchert [a], W. Borgs [a], M. Debowski [c], W. Erven [d], R. Esser [e,1], P. Fedorets [f], D. Gotta [a], M. Hartmann [a], V. Hejny [a], A. Kacharava [g,h], H.R. Koch [a], V. Komarov [g], P. Kulessa [i], A. Kulikov [g], G. Macharashvili [g,h], S. Merzliakov [g], S. Mikirtychiants [b], H. Müller [c], A. Mussgiller [a], R. Nellen [a], M. Nioradze [h], H. Ohm [a], A. Petrus [g], F. Rathmann [a], Z. Rudy [i], R. Schleichert [a], Chr. Schneider [c], O.W.B. Schult [a], H.J. Stein [a], I. Zychor [j]

[a] *Institut für Kernphysik, Forschungszentrum Jülich, 52425 Jülich, Germany*

[b] *High Energy Physics Department, Petersburg Nuclear Physics Institute, 188350 Gatchina, Russia*

[c] *Institut für Kern- und Hadronenphysik, Forschungszentrum Rossendorf, D-01474 Dresden*

[d] *Zentralinstitut für Elektronik, Forschungszentrum Jülich, 52425 Jülich, Germany*

[e] *Institut für Kernphysik, Universität zu Köln, Zülpicher Str. 77, 50937 Köln, Germany*

[f] *Institute for Theoretical and Experimental Physics, Cheremushkinskaya 25, 117259 Moscow, Russia*

[g] *Laboratory of Nuclear Problems, Joint Institute for Nuclear Research, 141980 Dubna, Russia*

[h] *High Energy Physics Institute, Tbilisi State University, University Street 9, 380086 Tbilisi, Georgia*

[i] *Institute of Physics, Jagellonian University, Reymonta 4,30059 Cracow, Poland*

[j] *The Andrzej Soltan Institute for Nuclear Studies, 05400 Swierk, Poland*

Abstract

The spectrometer ANKE has been put into operation at the accelerator COSY of the Forschungszentrum Jülich in spring 1998. An initial scientific goal is to study K^+-production in pA collisions at subthreshold energies far below the free NN-threshold at $T_p = 1.58$ GeV. This requires the identification of K^+-mesons in a background of pions and protons, about 10^6 times more intense. In this paper the sophisticated detection system and the software procedures for kaon identification are described. With the help of TOF, energy-loss and range measurements as well as the track information from wire chambers, it is possible to measure $\mathrm{d}^2\sigma/\mathrm{d}\Omega\,\mathrm{d}p$ for deep subthreshold K^+ production at beam energies down to $T_\mathrm{p} = 1.0$ GeV.

PACS: 29.40.-n; 25.40.-h

Key words: K^+-meson detection; Subthreshold K^+-production

1 Introduction

The production of K^+-mesons in proton-nucleus reactions at beam energies below the free nucleon-nucleon threshold ($T_\mathrm{p} = 1.58$ GeV), so-called subthreshold production presently is a topic of strong interest [1–4]. Since K^+-mesons have a long mean free path in the nuclear medium it is expected that valuable information about short-range correlations in nuclei can be extracted from these studies. Further research goals are insights into the reaction dynamics, different production mechanisms and the properties of the produced kaons inside the nuclear environment. In a recent theoretical paper [3] it has been pointed out that the existing data still do not allow to draw unambiguous conclusions about the above mentioned issues. Differential spectra are needed in a wide momentum range for different target nuclei and beam energies. This is particularly the case at beam energies below 1.2 GeV since so far only total cross sections have been measured there [1].

The great challenge of kaon studies at beam energies far below the NN-threshold is the fact that the production cross sections are extremely small. Furthermore, the produced K^+-mesons have a short life time and, thus, a very compact detection system is mandatory, in particular at low kaon momenta. The magnetic spectrometer ANKE [5–10] and its detectors have been built and optimized for such measurements.

In order to get realistic estimates on the K^+ and background rates at ANKE, calculations were performed using the Rossendorf-Collision (ROC) model [11]. Figure 1 shows the result of these model calculations for proton-carbon collisions. The production cross sections shown in the figure are integrated over the angular range $\vartheta = 0\ldots10^\circ$ — roughly corresponding to the angular acceptance of ANKE [6,10]. It can be seen that the background of protons and

[1] Now working at: Saint-Gobain Crystals & Detectors GmbH, 42929 Wermelskirchen, Germany.

pions stays nearly constant whereas the kaon cross section dramatically decreases as the energy approaches the absolute threshold (T_p = 0.75 GeV for carbon); at $T_\mathrm{p} = 1.0$ GeV, the lowest energy of our measurements up to now, the K^+/π^+ ratio is as small as $\sim 10^{-6}$. Note that the cross sections presented in Fig. 1 are momentum integrated. Most of the produced protons are above the momentum range measured at ANKE. Thus, in the spectra presented in Sect. 3.1, the number of pions and protons is approximately equal. However, high-momentum protons can hit structure material, e.g., the pole shoes of the spectrometer magnet and produce secondary particles. In fact, those turned out to be the most severe source of background, see Sect. 3.2.

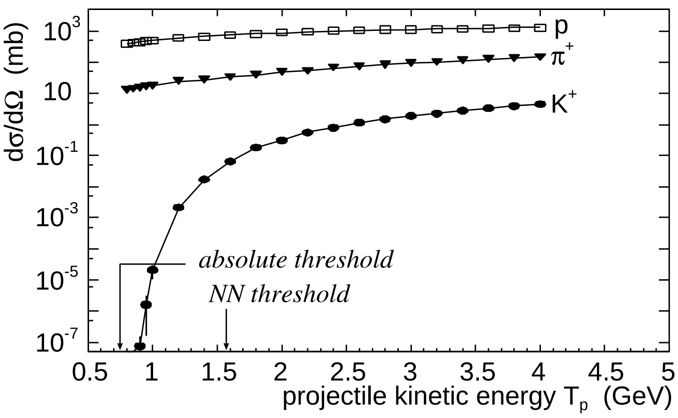

Fig. 1. Predicted momentum-integrated cross sections for the production of K^+ mesons and background particles in proton-carbon collisions into emission angles $\vartheta < 10°$. The calculations were made using the Rossendorf-Collision (ROC) model [11].

The spectrometer ANKE has been described in detail in [9]. Therefore, in this paper only a brief overview of the setup and its detection systems for K^+-mesons is given. The procedures for data analysis are described and it is shown how momentum distributions of kaons from proton-nucleus collisions at beam energies as low as 1.0 GeV are obtained.

2 Description of the experimental setup

2.1 Principles of K^+-Identification with ANKE

For the identification of K^+-mesons the following criteria are used at ANKE:

- ANKE provides a momentum focusing of the ejectiles (Sect. 2.2). This is used to define the K^+-momenta and serves as an important means to suppress the background of pions and protons in range telescopes (Sect. 2.3.2).

- A fast on-line trigger system based on start- and stop detectors of a time-of-flight setup allows the selection of particles with certain momenta and emission angles at the target. Narrow time-of-flight (TOF) gates can be defined for the identification of pions, kaons and protons, respectively (Sect. 2.3).
- Range telescopes in the focal surface of the spectrometer dipole discriminate pions, kaons and protons with the same momenta due to their different energy losses. Passive degraders in the telescopes between the scintillation counters enhance the discrimination efficiency (Sects. 2.3.2 and 3.1).
- The K^+-mesons are stopped in the range telescopes. Their decay with a lifetime of $\tau = 12.4$ ns provides an effective criterion for the identification of these mesons via the detection of delayed signals (Sects. 2.3.2 and 3.1).
- The tracks of the ejectiles are measured with multi-wire proportional chambers (MWPCs) (Sect. 2.3.1). From this information the emission angles at the target are deduced and a suppression of background not originating from the target is possible (Sect. 3.2).

2.2 The ANKE spectrometer

The ANKE spectrometer [7–10] is located at the internal target position TPA of the cooler synchrotron COSY-Jülich. It consists of three dipole magnets — two smaller ones (D1 and D3, see Fig. 2) to guide the circulating COSY beam and a C-shaped spectrometer magnet (D2) with a large gap height of 20 cm. Between D1 and D2, space for the installation of various internal targets is available. For the measurements described here, triangular-shaped foil targets made of carbon (polycrystalline diamond), copper and gold were suspended from frames [9]. The target dimensions typically are 2 mm (width at base glued to the frame), 20 mm (length) and 0.04–15 mg/cm^2 (thickness). D2 has an angular acceptance of $\Delta\Omega \approx 50$ msr for ejectiles emitted under forward angles $\vartheta \approx 0^\circ$. Furthermore, the flight path of the ejectiles between target and the focal-surface detectors is short ($l \approx 150 \ldots 400$ cm) so that kaons reach the detectors with a probability of ~ 30 % in spite of their short lifetime.

Each of the range telescopes located at the focal-surface was optimized for a certain kaon-momentum range, see Sect. 2.3.2. Therefore, when changing the beam energy to measure the K^+-momentum spectra for different projectile energies, one must keep constant *i)* the field in the ANKE magnets and *ii)* the relative locations of target and D2 so that the momenta of the ejectiles hitting a certain telescope remain constant. Consequently, the radius of curvature and the deflection angle of the circulating COSY beam changes in all three dipoles with varying beam energy. This can be compensated by a movement of the spectrometer dipole D2 perpendicular to the direction of the undisturbed COSY beam [9]. For the measurements described in this paper, all three magnets were operated at a fixed field strength of $B = 1.30$ T (measure-

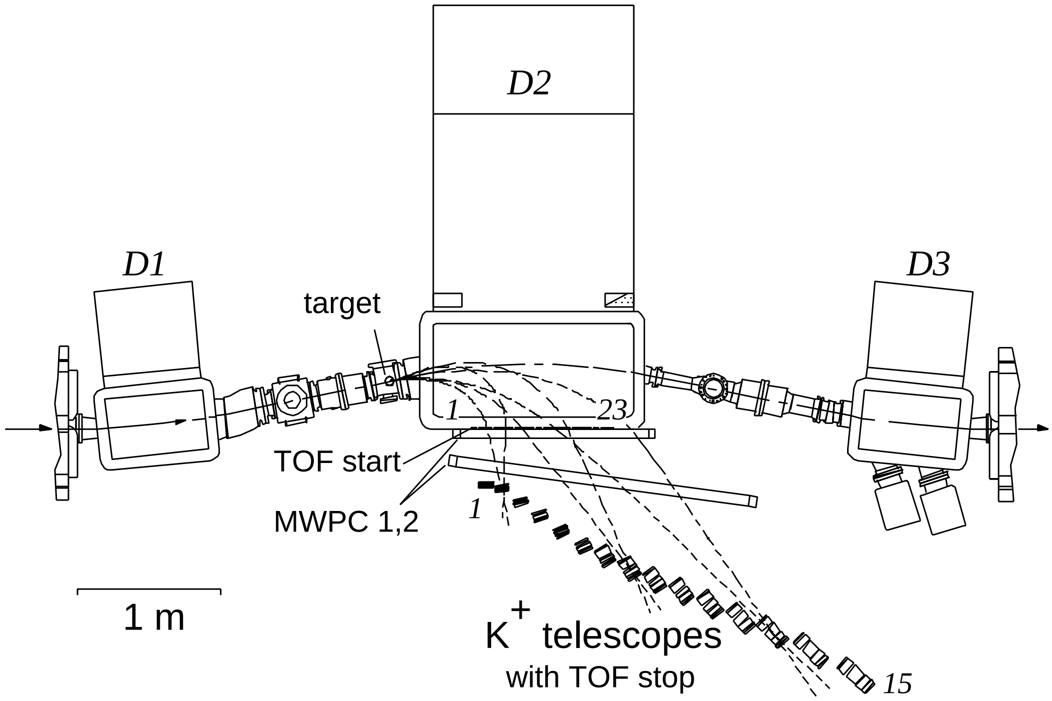

Fig. 2. Top view of the ANKE spectrometer and detectors used for K^+ identification. The dashed lines show trajectories of ejectiles with different momenta and horizontal emission angles of $\vartheta \pm 10°$. The numbers indicate the positions of the 23 start counters and the 15 telescopes.

ment of the K^+-production cross sections) or at the maximum achievable field strength in D2 of $B = 1.57$ T (calibration measurements for the time-of-flight detectors). The lower field strength used for the cross-section measurements was chosen in order to avoid too large deflection angles of the COSY beam at low beam energies. The resulting deflection angles in D1, $\alpha = 10.1° \ldots 5.5°$ at $T_\mathrm{p} = 1.0 \ldots 2.3$ GeV, are in any case smaller than the maximum value of $10.6°$ permitted by the bellows of the vacuum system, see [9] for details.

Ray-tracing calculations [10] show that at $B = 1.30$ T the K^+ telescopes cover a momentum range of $p \approx 110 \ldots 525$ MeV/c. The horizontal angular acceptance of D2 for which the focusing properties are still sufficient to allow kaon identification in the telescopes is $\vartheta \approx -15° \ldots +15°$, cf. Sect. 2.3. The vertical acceptance is given by the gap height of D2 and varies between $\phi \approx \pm 7°$ for the lowest momenta and $\pm 3.5°$ (highest). The heights of all detectors were chosen such that they cover the full vertical acceptance of the spectrometer dipole.

2.3 K^+-detection system

The schematic layout of the K$^+$-detection system at ANKE is sketched in Fig. 3. It is rigidly connected to the spectrometer dipole D2 and consists of three major components: *i)* 23 TOF-start counters (*PILOT-U, Nuclear Enterprises*) close to the vacuum window (made of 500 μm Al) at the right-hand side of D2. The counters are positioned as close as possible to the exit window in order to maximize the distance to the TOF-stop counters. Each start counter has a horizontal angular acceptance of $2° - 6°$ depending on the ejectile momenta. All scintillators are 27 cm high and 5 cm wide. Their thickness has been chosen as a compromise between sufficient light output and little small-angle scattering. It increases from 0.5 mm (counters 1, 2) for the low momentum detectors to 1.0 mm (counters 3—5) and 2.0 mm for higher momenta. Each scintillator is read out on both ends by a photomultiplier. *ii)* The tracking system to reconstruct ejectile trajectories consisting of two multi-wire proportional chambers (MWPC 1, 2). They are located in front of all detector components except the TOF-start counters in order to minimize distortions of the ejectile trajectories due to small-angle scattering. *iii)* 15 range telescopes which are placed along the focal surface of D2. The horizontal angular acceptance of each telescope varies from $\pm 1°$ to $\pm 15°$ depending on the on- or off-line coincidences with the corresponding start counters. Each telescope is composed of TOF-stop, ΔE, veto scintillation counters (*BC408, Bicron*), which are read out by photomultipliers on both sides, and two passive degraders made of copper. Telescopes 9–15 also contain lucite Čerenkov counters. For a detailed description of the telescopes see Sect. 2.3.2.

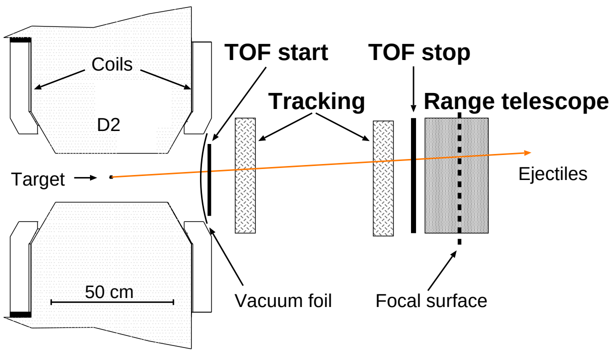

Fig. 3. Simplified layout of the detection system used for the subthreshold K$^+$-studies at ANKE (looking in the direction of the circulating COSY beam).

The precise time information from the start, stop, ΔE and veto counters (see Sect. 3.1 for values of the time resolution) is achieved by constant-fraction discriminators and mean timers both specifically developed for this purpose [12]. In addition, the vertical spatial information in each scintillator is obtained from the time difference of both phototubes. The resolution for the stop detectors is better than 30 mm (FWHM). With one specially built VME-module for each stop counter it is possible to set a common TOF gate (length variable between 3 ns and 23 ns) in coincidence with up to 16 individually adjustable start-stop combinations [12]. In this way corridors of acceptable start-stop combinations can be defined through which the K^+-mesons from the target should pass. A total of 16 VME modules is needed for the ANKE on-line TOF trigger which allows to select pions, kaons or protons already during data taking.

2.3.1 Multi-wire proportional chambers

The two MWPCs [13,14] of the ANKE K^+-detection system have been built in a modular design at the Forschungszentrum Rossendorf and differ only in the dimension of the sensitive planes and the diameter of the anode wires (see Table 1). The arrangement of the sensitive wires in the planes, vertical and inclined by $+30°$ and $-30°$, respectively, allows to determine the space coordinates of the particle track in the wire chamber. Together with the knowledge of the magnetic field of the D2 magnet one can reconstruct the momentum and emission angle of the particle at the target position. The necessary accuracy of the reconstructed momentum $\Delta p/p$ is 2–3% for pions. This can be achieved with a wire spacing of 2.54 mm. An intrinsic resolution $\sim$ 0.7 mm between the inclined and vertical planes has been determined in test measurements [13].

Table 1
Properties of MWPC 1 and MWPC 2.

	MWPC1	MWPC2
Gas mixture	70% Ar : 30% CO_2	
No. of anode planes	3	
Arrangement of anode wires	vertical and $+30°$ und $-30°$ inclined	
HV anodes	0 V	
max. HV cathodes	-3000 V	
Wire spacing	2.54 mm	
Distance anode-cathode	5 mm	
No. of wires per plane	512	768
Anode wires	20 μm tungsten	25 μm tungsten
Cathode material	18 μm mylar foil	23 μm mylar foil
Sensitive area	$35 \cdot 130$ cm^2	$60 \cdot 196$ cm^2

The readout of the chambers is performed using a highly integrated front-end system based on two chips which were developed at the Rutherford Appleton Laboratory (RAL) [15]. The analog chip RAL 118 amplifies and discriminates the signal. The digital chip RAL 111 on the one hand provides the proper delay of the signal using a digital shift register. This is necessary since the signal of the MWPCs must be stored until the system trigger has been generated. On the other hand, RAL 111 digitizes the signals and performs zero suppression. The latter leads to a huge data reduction since in a typical event only around 2% of the wires have a signal and only the numbers of those wires are sent to the subsequent data-aquisition system. Thus during the K^+-measurements particle fluxes of about 5000 s^{-1} per wire could be handled by the readout system. A more detailed description of the complete readout system can be found in [16].

The drift time of electrons in the used gas mixture is 80 ns at most [17]. Therefore no restrictions are expected when the chamber is operated at a maximal particle flux of 10^6 s^{-1}. To minimize the number of multiple hits the width of the readout gate is set to 110 ns.

2.3.2 The K^+ range telescopes

The K^+-telescopes are positioned along the focal surface of D2 perpendicular to the trajectories of ejectiles which leave the target in the forward direction, $\vartheta = 0°$. Each detector covers a limited momentum range given by its width of 10 cm and the dispersion of D2. The values for the momentum acceptances which are shown in the right column of Table 2 were calculated for ejectiles emitted at 0° from the target and neglecting small angle scattering in the vacuum foils and the detector components.

Figure 4a) shows momentum distributions for three telescopes which were obtained from data on π^+-production in proton-carbon collisions and from corresponding GEANT simulations. For the reconstruction of the pion momenta from the wire-chamber information, a simple box-field approach has been applied in which the trajectories in front of and behind the effective field of D2 are described by straight lines. The ejectile momenta are determined by calculating a circular arc with a constant radius of curvature connecting these straight lines. The fact that each of the telescopes is hit by ejectiles within a rather limited momentum range of $\Delta p/p = 7 - 24\%$, provided they originate from the target at angles less than $\sim 15°$ (see right column of Table 2), allows to exploit the different ranges and energy losses of ejectiles with different masses for the K^+-identification, see Sect. 3.1 for details.

Figure 4b) shows momentum distributions for telescope #13 and the individual start counters. It can be seen that particles which traverse start counters #10–21 have a small momentum spread, $\Delta p/p \approx 8\%$. The lowest counters also detect fast ejectiles which are emitted from the target at large angles $\vartheta \leq 30°$. Since they miss the well-defined field region of D2 they are only

Table 2
Dimensions of the telescope components used for the measurements at $B = 1.30$ T. In addition, telescopes #9–15 contain 5 cm thick lucite Čerenkov counters between stop and degrader I. The momentum ranges covered by each telescope are given in the last column.

	Height	Thickness [cm]					Momentum range
Telescope	[cm]	Stop	Degr.I	ΔE	Degr.II	Veto	[MeV/c]
1	52	0.3	—	0.5	0.2	1.0	110–140
2	57	0.5	—	0.5	0.2	1.0	140–160
3	62	1.0	—	1.0	0.2	1.0	160–182
4	67	1.0	—	1.0	0.8	1.0	182–205
5	77	1.0	0.1	1.5	0.8	1.0	205–227
6	82	1.0	0.11–0.37	2.0	0.8	1.0	227–252
7	88	1.0	0.26–0.58	2.0	1.6	1.0	252–280
8	94	1.0	0.43–0.82	3.0	1.3	1.0	280–310
9	100	1.0	0.11–0.57	3.0	1.0	1.0	310–340
10	100	1.0	0.49–1.08	3.0	1.5	1.0	340–370
11	100	1.0	1.06–1.78	3.0	1.7	1.0	370–400
12	100	1.0	1.70–2.57	4.0	1.0	1.0	400–430
13	100	1.0	2.56–3.49	4.0	1.0	1.0	430–460
14	100	1.0	3.23–4.34	5.0	2.0	1.0	460–490
15	100	1.0	4.20–5.37	5.0	2.0	1.0	490–525

slightly deflected so that their momentum distributions smear out. Indicated in the figure is the range of valid start counters which are accepted by the on-line TOF trigger. For these counters, corresponding to horizontal emission angles $|\vartheta| \leq 12°$, the imaging properties of D2 are sufficient to detect ejectiles with well defined momenta.

The telescopes consist of vertically oriented scintillators and copper degraders. The thicknesses of all components were determined with the help of GEANT simulations [17,18] for K^+-identification. The results of the simulations were verified for a sample telescope by test measurements with pion, kaon and proton beams from the 10 GeV proton synchrotron at ITEP, Moscow [4]. Table 2 shows the thicknesses of all components used during the measurements described here. The first counter in each telescope is the TOF-stop counter, see Fig. 5, followed by 5 cm thick lucite Čerenkov counters (in telescopes #9–15 only) for the suppression of fast pionic and leptonic background. During data analysis it turned out that these counters provide no additional back-

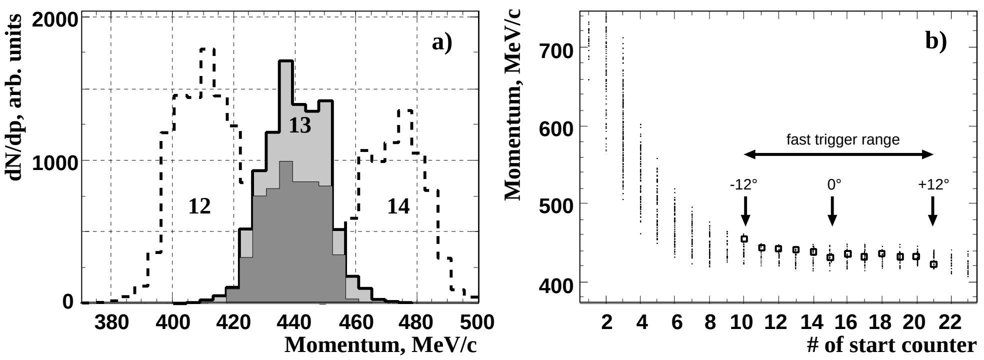

Fig. 4. **a)** Momentum distribution of pions from p(2.3GeV)C $\to \pi^+$X reactions emitted at angles $\leq 10^\circ$ and detected in telescopes #13 (light shaded histogram), 12 and 14 (dashed). For comparison the result of a GEANT simulation is given (dark shaded, scaled down by an arbitrary factor). **b)** Simulated momentum ranges for the individual start counters and telescope #13. For the simulation horizontal emission angles of even up to 30° were permitted. The central arrow indicates the start counter which detects particles emitted at 0° at this setting of the beam energy and field strength in D2; the range of start-stop combinations accepted by the fast trigger is indicated by the horizontal bar. Also shown by the open squares are the mean ejectile momenta calculated from TOF spectra, see Sect. 3.1 for details.

ground suppression. Thus they were not used in the current analysis for kaon identification.

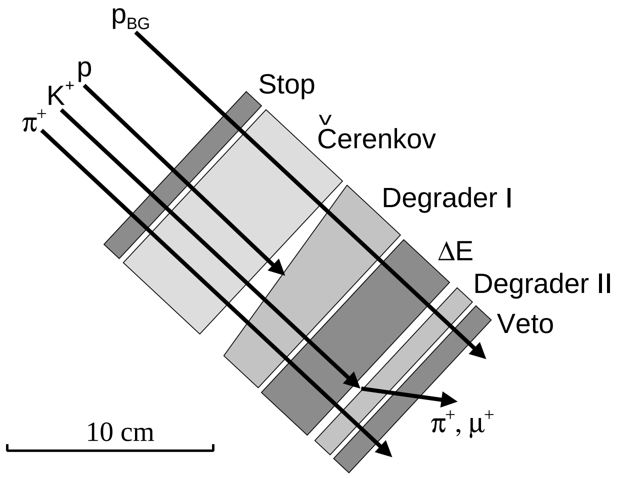

Fig. 5. Sketch of telescope #13. The ranges of pions, kaons and protons originating from the target as well as scattered protons (p_{BG}) with the same velocity (i.e. TOF) as kaons are indicated. See text for a detailed description of detector components.

The function of degrader I is twofold: first, it stops protons originating from the target and prevents them from entering the ΔE counter. Second, it slows down kaons such that they are stopped at the far end of the ΔE counter or in the second degrader. This results in a large K$^+$ energy loss in the ΔE counter which helps to separate them from pions and scattered protons, see Sect. 3.1. The tapered shape of degrader I accounts for the momentum dispersion along the focal surface of D2: From the left to the right edge of each telescope the degrader thickness increases in correspondence with the ejectile momentum. In order to minimize the range spread for kaons, each telescope is positioned such that the first degrader is located in the focal plane where the momentum spread of the ejectiles is smallest. Pions from the target pass through the counters and degraders almost unaffected due to their high velocity and result in small energy losses in all counters. The thicknesses of degrader I have carefully been fine tuned during calibration measurements (by adding thin copper sheets) at $T_{\rm p} = 2.3$ GeV where the kaon rate is sufficiently high to identify them without the help of the energy-loss spectra in the ΔE counter, see Sect. 4.

Kaons which are stopped in the ΔE counter or in the second degrader decay with a lifetime of $\tau = 12.4$ ns. Their decay products, μ^+ or π^+ emitted isotropically, can reach the veto counter and result in signals which are characteristically delayed with respect to K^+-signals in the stop or ΔE counters of the same telescope. This provides an additional criterion for K^+-identification which becomes particularly important for low beam energies. This method based on the detection of delayed decay muons was already applied previously in the measurement of total cross sections at beam energies between 0.8 and 1.0 GeV [1].

The most problematic background is caused by secondary protons produced on the pole shoes of D2 or in the vacuum chamber. This contains a component with the same time-of-flight as the kaons and thus approximately twice their momenta. Such protons ($\rm p_{BG}$), which are also indicated in Fig. 5, pass through all detectors of a telescope. The thicknesses of degrader II were chosen larger than necessary to prevent kaons from reaching the veto counter: they also slow down the background protons such that their energy loss in the veto counter significantly increases beyond that of the koan-decay products. Selection of events with small energy losses in the veto counters thus is an additional criterion for kaon identification since their decay muons and pions are minimum ionizing.

3 Data analysis

3.1 Examples of scintillator spectra

Examples of time-of-flight (TOF) distributions between the stop counter of telescope #13 and the different start counters are shown in Figure 6. The data were taken during a calibration run with high field strength in D2 ($B = 1.57$ T). During data taking an open on-line TOF trigger was chosen such that pions, protons and scattered particles are visible in the spectra. Most of the spectra show two distinct peaks for pions and protons originating from the target which have well defined momenta, $p \approx 430 - 460$ MeV/c, see Table 2 and Fig. 4. From the spectra an average time resolution of ~ 650 ps (FWHM) for target pions in the central region — start counters #10–21, corresponding to horizontal emission angles $|\vartheta| \leq 12°$ — has been deduced. The shift of the proton peaks towards smaller flight times and the larger width ($\sim$ 1000 ps) for the lower start-counter numbers is due to the momentum spread shown in Fig. 4b) which causes a variation of the proton velocities. This is not the case for pions since, due to the low mass, their velocity is close to the speed of light. For start-counters with numbers below 5, the two peaks disappear and a broad TOF distribution develops because of the high-momentum protons, see Fig. 4b). The pions are suppressed here because of inefficiencies of the first few start counters for high momentum pions. In start counter #23 the peak of protons from the target is reduced for the following reasons: the average ejectile momenta (and ranges) are smaller, see Fig. 4b), and the effective counter thickness is increased due to the smaller entrance angle into the telescope. This prevents part of the target protons from reaching the ΔE counter. Since a signal in this counter was required in the on-line trigger only the fastest protons can be detected and the proton rate is reduced. This effect also has an influence on the spectra of start counters #18–21. Here the width of the proton peak is reduced from 1000 ps down to 500 ps.

The separation of the pion- and proton-TOF peaks in Fig. 6 allows to calculate the average momentum of the ejectiles originating from the target. The deduced values for start counters #10–21 are presented as the open squares in Fig. 4b) and agree with the momenta from ray-tracing calculations using GEANT. Remember that the TOF spectra from Fig. 6 were obtained at a field strength of $B = 1.57$ T in D2 (field setting used for the TOF calibrations) whereas the momentum ranges in Fig. 4 are given for $B = 1.30$ T (field setting used for the cross-section measurements). Thus the momenta from TOF were multiplied by the ratio of the field strengths 1.30/1.57 in order to allow a comparison with the GEANT simulations.

Fig. 7 shows the energy-loss spectra which were measured simultaneously with the TOF spectra of Fig. 6. They allow to determine the detection efficiencies for pions in the start counters assuming that the energy-loss distributions can be fitted by Landau distributions. Values of $\sim$ 95% were obtained, except for the first two start counters which are only 0.5 mm thick. In this case the efficiencies are below 50%. For kaons the detection efficiencies are higher and very close to 100%. The efficiencies are taken into account when normalizing the number of identified kaons to known pion-production cross sections.

Figure 8a) shows the combined TOF distribution for the stop counter of telescope #13 and start counters #10–21 from Fig. 6. The time resolution for

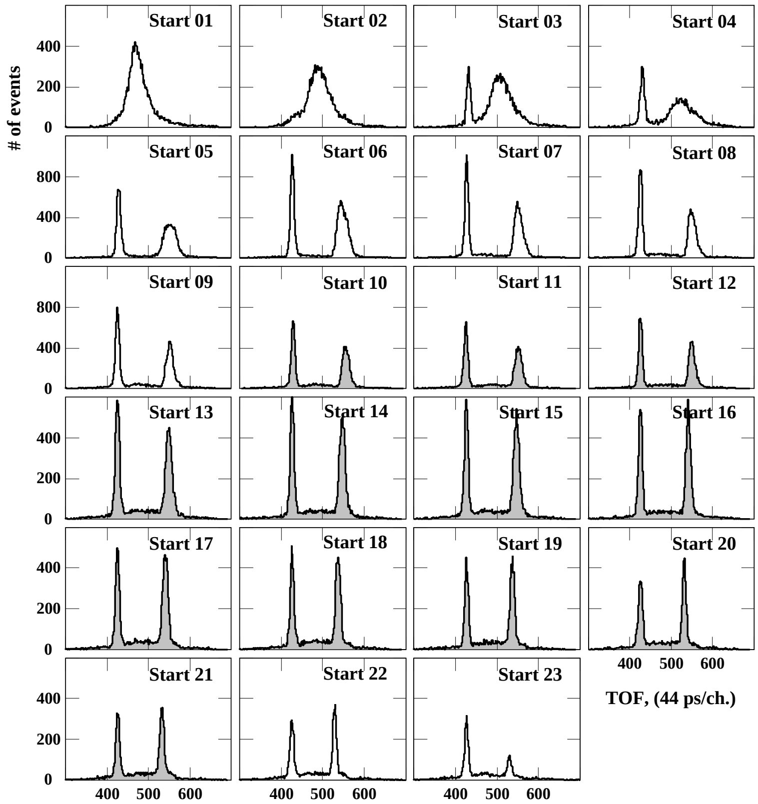

Fig. 6. Time-of-flight spectra at an incident proton energy $T_{\mathrm{p}} = 1.5$ GeV between stop counter #13 and start counters # 1–23. The data presented in this figure were obtained during a dedicated calibration run with open trigger at $B = 1.57$ T with a carbon target. The range of "valid" start counters for this particular stop counter, see Fig. 4b), is indicated by the shaded histograms.

pions in Fig. 8a) amounts to 650 ps (FWHM), as in case of the individual spectra from Fig. 6. Due to the different lengths of the flight paths for each start counter, the values of the TOF difference between pions and protons vary, which causes a smearing of the proton peak in the sum spectrum.

In principle, the observed time resolution should allow a clear separation of pions (protons) and kaons. The TOF difference between pions and kaons (peak-to-peak) amounts to $\sim 8\sigma$; assuming a pure gaussian distribution one would expect a pion suppression much better than the requested 10^6. Such a huge suppression is, however, not achieved in the experiment due to background produced in secondary hadronic interactions. The flat background in Fig. 8 is mainly caused by fast protons emitted from the target at small angles. These protons can hit the pole shoes of D2 or structure material of the vacuum chamber and produce secondary particles which then can reach the telescopes. Such secondary particles are not focussed by D2 and, hence, do not have well defined momenta. Therefore, they result in a broad background distribution in the TOF spectra. Indicated by the shaded area in the sum spectra of Fig. 8 and the following ones are the regions where kaons are expected. This serves

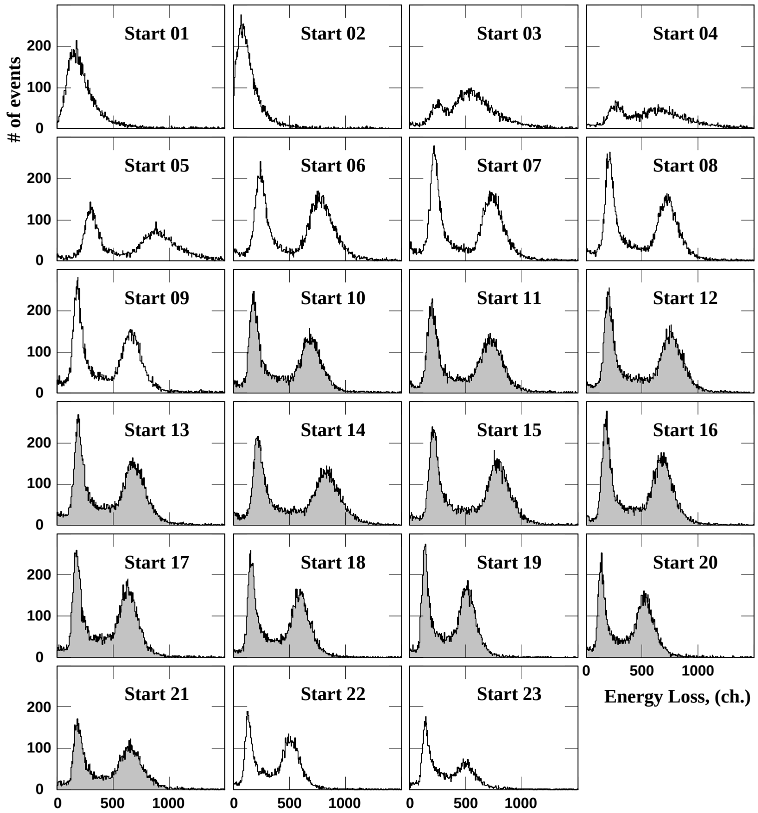

Fig. 7. Energy-loss spectra for the same start-stop combinations as in Fig. 6.

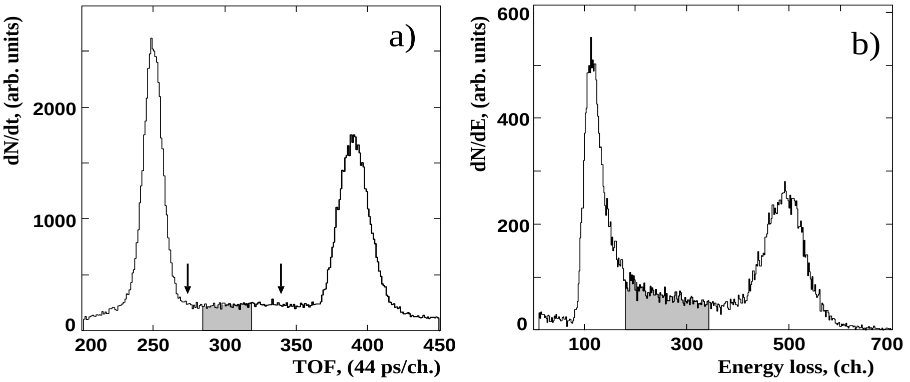

Fig. 8. **a)** TOF and **b)** amplitude spectra of stop counter #13 in coincidence with start counters # 10–21. The approximate position of the gates for the off-line kaon identification are indicated by the shaded areas (see text). Arrows mark the narrowest TOF gates used for on-line event selection. The data were obtained at $B = 1.57$ T with a carbon target.

for illustration only since in the process of kaon identification, individual gates were used for each start-stop combination (i.e. spectra in Fig. 6). The same applies for *all other* scintillator time and amplitude spectra.

Figure 8b) shows the energy-loss distribution in stop counter #13 for ejectiles detected in coincidence with start counters #10–21. As for the TOF spectrum of Fig. 8a) the raw spectrum shows two peaks from pions and protons from the target and a broad background distribution. The ratio of the energy losses of protons and pions is ~ 4.5 as expected from the Bethe-Bloch formula. Consequently, only a moderate separation of pions and kaons (expected energy-loss ratio ~ 1.7) can be achieved from the amplitude signals. Since the lower edge of the pion energy-loss distribution is clearly visible in Fig. 8b), the detection efficiency for pions is larger than 98%. The same high efficiency has been obtained for kaons since the gate indicated in the figure is rather wide.

Figure 9a) shows the energy-loss distribution in the ΔE counter of telescope #13. The data were obtained at $B = 1.30$ T. Since protons from the target are stopped in the Čerenkov counter or in the first degrader there is only one peak from target pions and a broad background distribution from secondary particles visible in the spectrum. As explained in Sect. 2.3.2, the first degraders are used to optimize the energy loss of kaons in the ΔE counters. The solid histogram in Fig. 9b) shows the corresponding energy-loss spectrum for kaons (identified as described later in Sect. 3.4). During the measurements it has been checked whether slight modifications of the degrader thicknesses can improve the kaon-to-background separation. For this purpose the kaon energy loss should be as large as possible (better separation from target pions), while keeping the width of the distributions small (optimization of the kaon to scattered-background ratio). It turned out that the optimization procedure for most telescopes resulted in thicknesses at which the kaons pass through the ΔE counter and are stopped in the second degrader. As an example the corresponding distribution is shown by the dashed histogram in Fig. 9b).

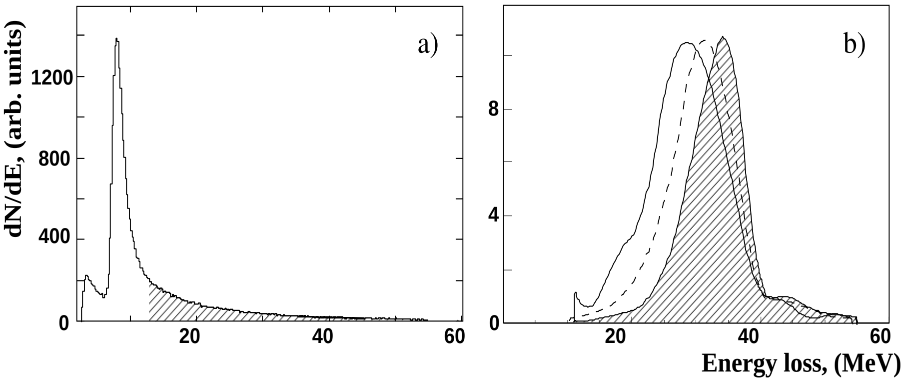

Fig. 9. Energy-loss spectra for ΔE-counter #13 in coincidence with start counters #10–21. **a)** Raw spectrum, the gate for kaons is located above $\Delta E \sim 13$ MeV. **b)** Kaon spectra taken during optimization of degrader I. The values of the tapered degrader thickness are: *i)* 2.76–3.69 cm (solid histogram, initial value from simulation calculations), *ii)* 2.66–3.59 cm (dashed histogram), and *iii)* 2.56–3.49 cm (shaded histogram, optimum thickness given in Table 2). All data were obtained at $T_{\rm p} = 2.0$ GeV and $B = 1.30$ T with a carbon target.

As explained in Sect. 2.3.2, the time information from the veto counter is a particularly effective criterion for kaon identification. If the kaons are stopped in the second degrader one expects that only their decay muons and pions can reach the veto counter with a time delay characteristic for the K^+-lifetime of 12.4 ns. Figure 10 shows the distribution of the time difference of particle detection in the veto and stop counters of telescope #13. One can clearly see a peak from particles directly passing through the second degrader (pions and secondary protons). In addition, there are delayed events visible which can be attributed to the decay products of K^+-mesons stopped in the second degrader, see Sect. 3.4. The on-line trigger for the accumulation of the K^+-data at low projectile energies rejected prompt events and admitted only those with a delay > 1.3 ns (channel 30). Off line a threshold of > 2.3 ns (channel 55) was set.

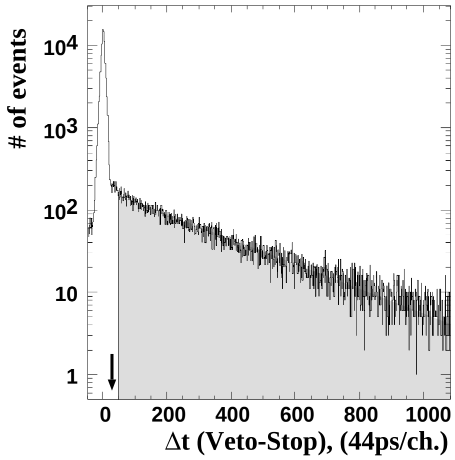

Fig. 10. Time difference between detection of particles in veto- and stop counter of telescope #13. To make the spectrum more illustrative, kaon gates were applied in the scintillator spectra described above and only particles were accepted which vertically come from the target plane (see next section). The arrow shows the location of the gates used during the measurements whereas the off-line cut is indicated by the shaded area, see text for details. The data were obtained at $T_{\mathrm{p}} = 2.3$ GeV and $B = 1.30$ T with a carbon target.

The use of the full scintillator information (TOF, energy loss in start, stop, ΔE and veto counters plus selection of delayed events in the veto counter) allows for a clear separation of the kaons from pions and protons originating from the target even at the lowest beam energy $T_{\mathrm{p}} = 1.0$ GeV. However, the background from secondary particles scattered at the pole shoes of D2 cannot sufficiently be suppressed. This is only possible by using the information from the wire chambers on the direction of the ejectiles as explained in the following section.

As indicated in Fig. 11 by the dashed line, particles from the target within the angular acceptance passing through the first MWPC at some vertical coordinate y are expected to have a certain vertical angle ϑ (which is measured with the second chamber). All ejectiles undergo multiple scattering in the vacuum foil of D2 and in detector components. This causes some smearing $\Delta\vartheta$ of the expected vertical angular distributions of particles from the target, for example $\Delta\vartheta_{\mathrm{K}^+}$. In contrast to target ejectiles, scattered protons p_{BG} in general have larger angular differences $\Delta\vartheta \mathrm{p}_{\mathrm{BG}}$. Thus the vertical MWPC information can very efficiently be used for the suppression of scattered particles.

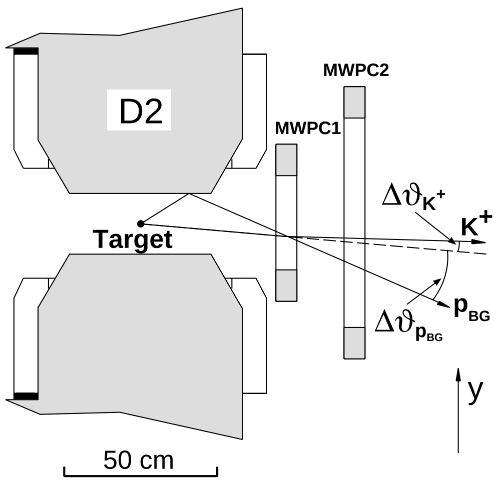

Fig. 11. Ejectiles from the target and scattered background in general have different vertical angles behind the spectrometer. See text for details.

Fig. 12 shows the vertical angular distributions $\Delta\vartheta$ for the remaining K^+-candidates after applying all cuts in the scintillator spectra described above. At the highest beam energy shown in the figure, $T_{\mathrm{p}} = 2.0$ GeV, there is a clear peak around $\Delta\vartheta = 0$ corresponding to ejectiles from the target. These particles can be identified as kaons, see Sect. 3.4. Only very few events from background particles are still visible. With decreasing beam energy the background surviving the scintillator cuts becomes significantly more important. The broad bumps at both sides of the target peak are mainly from ejectiles scattered at the pole pieces of D2 whereas background events underneath the peak must originate from the same vertical plane in which the target is located. The spectra from Fig. 12 are, for illustration, summed over all valid start counters. However, for identification of the K^+-mesons and for background suppression, the gates around the peak at $\Delta\vartheta = 0$ were optimized for each individual start-stop combination. It will be shown in Sect. 3.4 that for $T\mathrm{p} = 1.0$ GeV the remaining background underneath the peak is smooth and can be subtracted in order to determine the number of kaon events in each telescope. This is particularly important for measurements far below threshold.

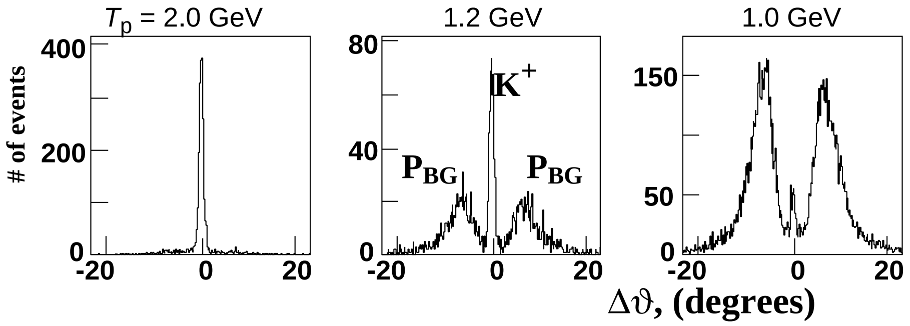

Fig. 12. Distribution of vertical angles measured with the two MWPC's after applying the K^+-cuts in the scintillator spectra of telescope #11. The spectra show a clear peak of kaons originating from the target. Background from scattered particles is also visible. The spectra were measured with a carbon target at three different beam energies.

In addition to the cuts on the vertical distributions from Fig. 12, in the horizontal direction (vertically oriented wires) events are only accepted if the responding wires are inside a corridor defined by trajectories connecting the edges of the individual start and stop counters. This criterion further helps to suppress scattered background, accidental coincidences and chamber noise. The width of these allowed corridors typically is 40. . . 100 wires (10. . . 25 cm).

3.3 Effectiveness of different criteria

In this section we briefly summarize the effectiveness of the most important cuts presented in Sects.3.1 and 3.2 for beam energies $T_p = 1.0$ and 2.3 GeV. At 2.3 GeV an on-line trigger based only on the TOF information was used which reduces the background and, thus, the amount of data written to tape, by about one order of magnitude. All other criteria, including narrower TOF gates, were applied off-line. The efficiencies of these criteria are summarized in Table 3.

At $T_p = 1.0$ GeV the background-to-kaon ratio is much larger than at 2.3 GeV. Thus, a stronger on-line trigger, based on TOF measurements and the (delayed) time signal from the veto counters, was used which drastically reduces the amount of data written to tape. During the off-line analysis subsequently stronger criteria were applied. In some cases two criteria were applied at the same time so that the combined efficiencies are shown in the table.

Table 3
Effectiveness of the individual cuts for T_p = 2.3 GeV. The numbers presented in columns "K^+" and "B.g." are the probabilities that K^+-mesons or background particles, accepted by the preceding criteria, are within the gate corresponding to the criterion described in the first two columns of the same line. (†for kaons with emission angles $|\vartheta| \leq 12°$; *see Fig.18 for efficiencies of the individual telescopes)

Criterion	Shown by	K^+	B.g.
Valid start counters (on-line)	Shaded spectra in Fig.6	$1.0^\dagger$	0.25
TOF (on-line)	Arrows in Fig.8a)	1.0	0.11
TOF (off-line)	Shaded area in Fig.8a)	0.99	0.29
Vertical direction	Fig.12	0.99	0.11
Delayed veto	Shaded area in Fig.10	0.2^*	$< 10^{-3}$
All		0.2	$< 3.5 \cdot 10^{-6}$

Table 4
Same as Table 3 for $T_\mathrm{p} = 1.0$ GeV.

Criterion	Shown by	K^+	B.g.
Valid start counters (on-line)	Shaded spectra in Fig.6	$1.0^\dagger$	0.25
TOF & delayed veto (both on-line)	Arrows in Fig.8a) Arrow in Fig.10	0.22	0.002
TOF (off-line) & vertical direction	Shaded area in Fig.8a) Fig.12	0.99	0.002
Delayed veto (off-line)	Shaded area in Fig.10	0.92	0.3
Narrower TOF cuts & Amplitude in ΔE counters	See Sect.3.4 Shaded area in Fig.9a)	0.6^*	0.05
All		0.12	$6 \cdot 10^{-8}$

3.4 Identification of K^+-mesons

Figure 13 shows the remaining events when analysis gates are set on *i)* TOF between start- and stop counters (Fig. 6), *ii)* amplitude information of all scintillation counters (e.g. Figs. 7, 8b, 9), *iii)* time difference between veto- and stop counters of one telescope (Fig. 10) and *iv)* MWPC information (Fig. 12). Due to the moderately large cross sections for kaon production at T_p = 2.3 GeV, clear peaks without background in the vertical-angle and TOF distributions are seen. The vertical-angle distribution (a) proves that the particles are directly coming from the target region and the TOF peak (b) is located at the position were kaons are expected. An exponential fit to the time distribution in the veto counters yields a value of $\tau = 12.0 \pm 0.3$ ns, consistent with the expected 12.4 ns.

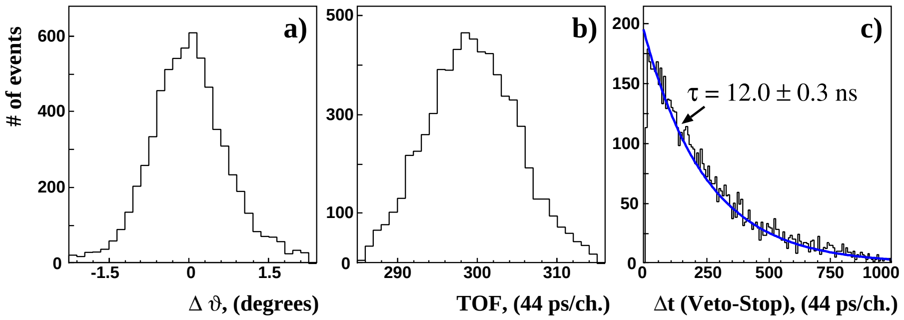

Fig. 13. **a)** Vertical angular distribution of K^+-events (c.f. Fig. 12). **b)**TOF distribution (c.f. Fig. 8a)). **c)** Time difference of detection in the veto and stop counters (c.f. Fig. 10); the spectrum has been shifted such that the gate for kaon detection is located at channel #0. All data were taken at $T_p = 2.3$ GeV with a carbon target. For illustration and in order to increase the number of events, the spectra shown in this section are summed over all valid start-stop combinations by properly shifting the distributions for each individual combination.

Figure 14 shows the same spectra as in Fig. 13 but now for the lowest beam energy, $T_p = 1.0$ GeV. Except for the beam energy, all other experimental conditions and software gates remain unchanged. Neglecting the now visible background, the location of the kaon distributions and, in the case of the vertical angle distributions, also the shape is the same as for the high energy where the production cross section is approx. 10^5 times larger.

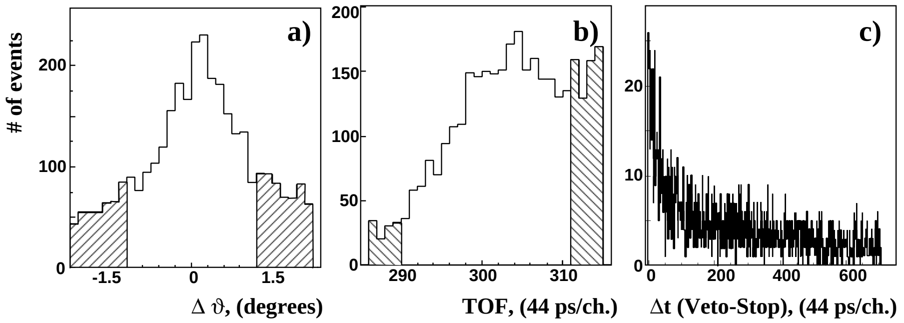

Fig. 14. Same as Fig. 13 but for $T_p = 1.0$ GeV. Indicated in **a)** and **b)** by the shaded areas are the angular and TOF cuts on background events which were used to determine the shape of the background distributions in Fig. 15.

In order to determine the number of detected kaons one has to subtract the background underneath the kaon peaks. The analyses show that this background has a smooth behaviour. As an example, in Fig. 15 the distributions of background events in the vertical-angle, TOF and $\Delta t(\text{veto} - \text{stop})$ spectra is shown. In particular, the vertical-angle distribution is constant in the region of the kaon peak and, thus, the background subtraction can be done by assuming a linear shape of the background in Fig. 14a).

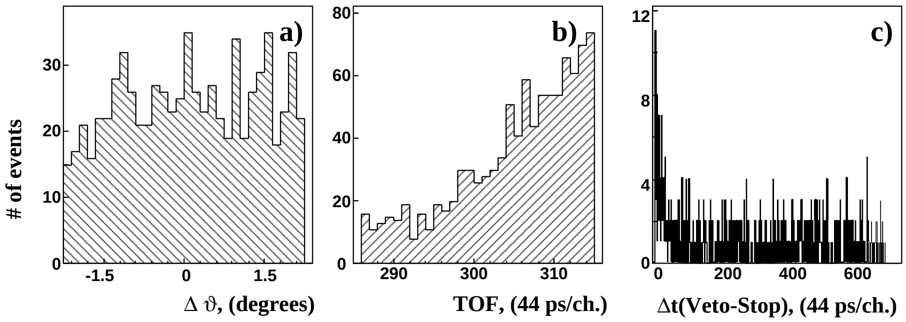

Fig. 15. **a)** Same as Fig. 14a) for background events within the outside gates of the K$^+$-TOF distribution from Fig. 14b). **b)** Same as Fig. 14b) for background events at the sides of the angular distribution from Fig. 14a). **c)** Same as Fig. 14c) for the events from a).

The remaining kaon distributions after background subtraction are shown in Fig. 16. Both the width of the TOF distribution as well as the exponential slope in the veto counter agree with the (clean) data at $T_{\mathrm{p}} = 2.3$ GeV.

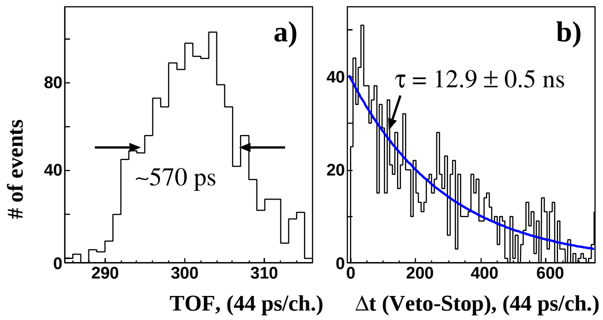

Fig. 16. Same as Fig. 14b) and c) after background subtraction.

4 K$^+$-momentum spectra

It has been shown in the previous sections that, after applying all criteria on TOF, energy losses and the MWPC information, K$^+$-mesons can be identified even at $T_{\mathrm{p}} = 1.0$ GeV. From the number of observed kaons in each telescope one can deduce momentum spectra, since the telescopes are placed along the focal surface of the spectrometer dipole. In order to obtain the double differential cross sections $\mathrm{d}^2\sigma/\,\mathrm{d}\Omega\,\mathrm{d}p$ for K$^+$-mesons produced at $\vartheta \sim 0°$, the kaon-detection efficiencies in each telescope have to be corrected for. The cross sections can then be obtained by normalizating to the number of identified π^+-mesons, which were measured in parallel, and to the known π^+-production cross sections. Further corrections, like e.g. for the different solid angles covered by each telescope and the acceptance gaps between them, are not necessary since they are identical for pions and kaons.

At ANKE, we have the possibility to directly determine the K$^+$-detection efficiencies in the telescopes through measurements at high beam energy, $T_p = 2.3$ GeV. Due to the rather large kaon-production cross section, it is sufficient to use for K$^+$-identification the TOF and the MWPC information *only*. Under these conditions, the efficiencies for kaon (and pion) detection result from the efficiencies of the involved detetors (TOF-start and -stop, MWPC's) which are well known and close to 100%, see Sect. 3. The upper spectra of Fig. 17 show the vertical-angle and TOF distributions of the events fulfilling these criteria. In both cases a peak of kaon events can be seen on top of a flat background distribution. The shape of this background has been determined in independent analyses: *i)* The data taken at 1.0 GeV were used where the cross sections are so small that, with the TOF/MWPC gates, "contaminations" from kaons can be neglected. *ii)* Events from the sides of the kaon distributions were used, see shaded areas of Fig. 14. In both cases the background distributions are almost linear. However, for background subtraction, different background shapes were taken into account and the uncertainties have been included into the errors for the detection efficiencies.

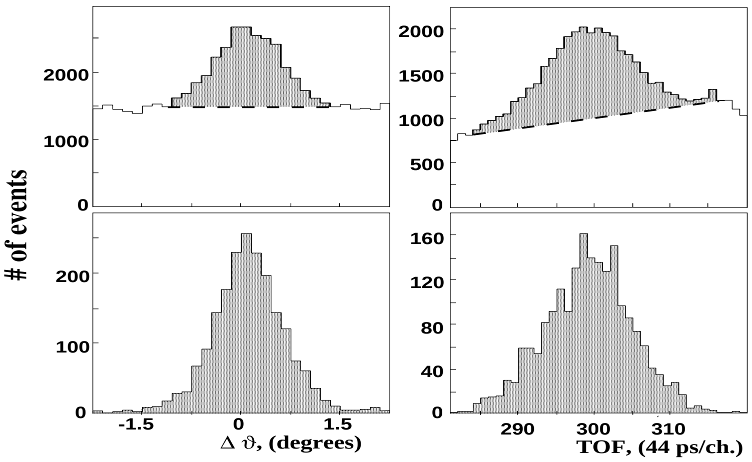

Fig. 17. Same as Fig. 13a) and b) but for telescope #13 only. Upper spectra: gates on TOF and vertical angles only (the gate widths correspond to the ranges of the two histograms). The background is indicated by the solid lines. Lower spectra: all criteria for K$^+$-identification applied (as in Fig. 13). The number of entries in the histograms cannot directly be compared to Fig. 13 since a different data set was used.

The lower spectra in Fig. 17 show the remaining K$^+$-events when *all criteria* (same as used in Sect. 3.4) for kaon identification are applied. In case of telescope #13, shown in the figure, approximately 10% of the kaons "survive" the cuts. The efficiencies — which are equal to the ratio of identified kaons with full gates and TOF/MWPC gates only — could be determined for telescopes 3–15. The corresponding numbers are shown in Fig. 18a) (for the first two telescopes the high background level of scattered particles does not permit to identify kaons with the TOF/MWPC gates only). The detection effiencies are in range of $\sim 10 \ldots 30\%$. The main kaon losses are due to a probability of only about 30% that a decay muon or pion enters the veto counter (limited solid angle), to kaon-scattering out of the telescopes in the first degrader and to hadronic interactions in the telescopes. The decreasing efficiency from telescopes #6 to #15 is caused by increasing thicknesses of the detectors and degraders. The step between #8 and #9 is due to the Čerenkov counters installed in telescopes #9–15; between telescopes #12 and #13 there is, for technical reasons, a significant increase of the distance between the ΔE and veto counters. In the lowest telescopes higher thresholds in the ΔE counters had to be used for kaon identification in order to suppress scattered background which leads to decreasing efficiencies.

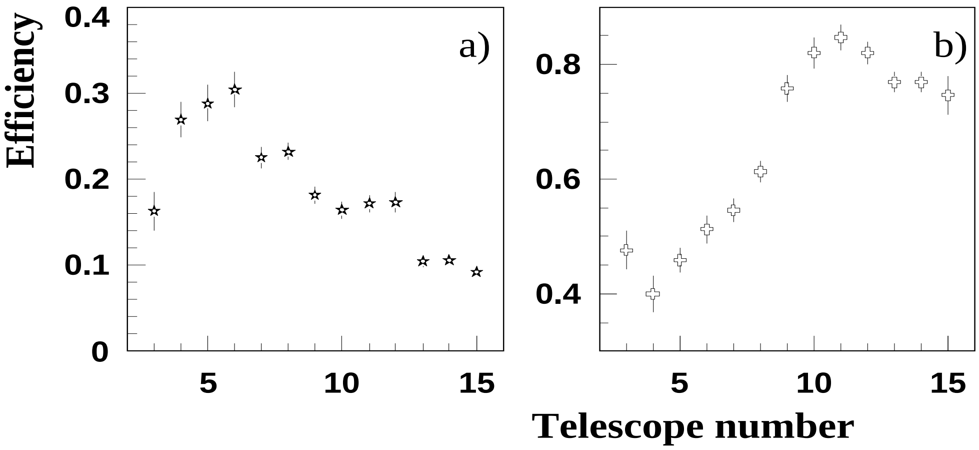

Fig. 18. **a)** Measured K$^+$-detection efficiencies in the individual telescopes. **b)** Correction factors which take into account the losses of K$^+$-counts due to the narrow TOF and energy-loss gates used in the off-line analysis at 1.0 GeV.

The cuts set on the spectra in the analysis of the data obtained at the lowest projectile energies were narrower than those for $T_{\rm p}$ = 2.3 GeV in order to suppress background as efficiently as possible. This leads to an additional loss of kaon events. Consequently, the obtained numbers of kaons at low energies also have to be corrected for the efficiencies shown in Fig. 17b) which were determined through a comparison of the numbers of identified K$^+$-mesons at 2.3 GeV with wide and narrow TOF and energy-loss gates.

Figure 19 shows the number of identified K$^+$-mesons in each telescope corrected for the efficiencies from Fig. 18. Except for the above mentioned corrections for decay-in-flight and the different momentum bites and solid angles covered by the individual telescopes, the spectrum shown in the figure is proportional to the double-differential cross section $\mathrm{d}^2\sigma/\mathrm{d}\Omega\mathrm{d}p$ for kaons produced in p(1.0GeV) $+^{12}$ C $\rightarrow$ K$^+$X reactions and emitted into forward angles $\vartheta \leq 12°$.

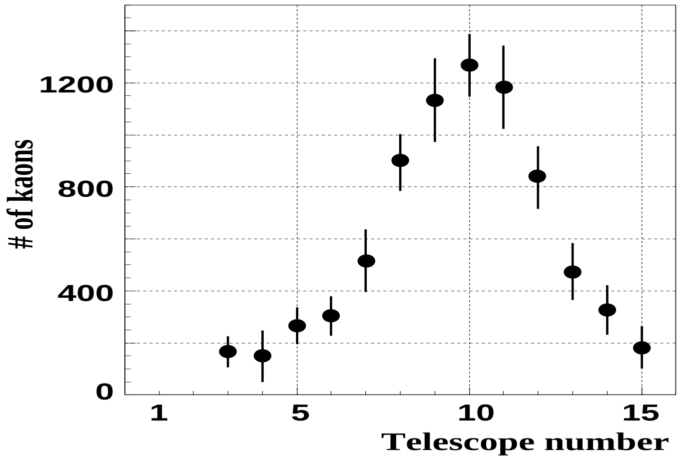

Fig. 19. Momentum distribution of K^+-mesons produced in a carbon target at $T_p = 1.0$ GeV. The numbers are not corrected for losses from decay-in-flight between target and stop counters and the different momentum bites of the telescopes (see Table 2). The error bars include the statistical uncertainties as well as the ones from the telescope-efficiency calibration.

5 Outlook

First measurements of K^+-momentum distributions in pA collisions at emission angles around 0° have been performed with the ANKE spectrometer at beam energies in the range $T_p = 1.0 \ldots 2.3$ GeV. It has been shown that ANKE and its K^+-detection system allow to identify the kaons out of a 10^6 times higher background of pions, protons and scattered particles. In order to extract double differential cross sections from the number of identified kaons shown in Fig. 19, one still has to correct for decay-in-flight between target and stop counters (30 to 36% of the kaons reach the counters) and the different momentum bites covered by the telescopes. Absolute normalization of the cross sections will be obtained from a comparison of π^+-data taken at ANKE with known π^+-production cross sections [19,20]. The results of the corresponding analysis procedures will be presented in forthcoming publications.

Acknowledgements

We would like to acknowledge the support we received for performing these first measurements at the ANKE spectrometer. The COSY-accelerator crew did an excellent job during beam-preparation and the experiments. Financial support from the following funding agencies was of indispensable help: Georgia (Department of Science and Technology), Germany (BMBF: grants WTZ-RUS-649-96, WTZ-RUS-666-97, WTZ-RUS-685-99, WTZ-POL-007-99; DFG: 436 RUS 113/337, 436 RUS 113/444, 436 RUS 113/561, State of North-Rhine

Westfalia), Poland (Polish State Committee for Scientific Research: 2 P03B 101 19), Russia (Russian Ministry of Science, Russian Academy of Science: 99-02-04034, 99-02-18179a) and European Community (INTAS-98-500).

References

[1] V.P. Koptev et al., *JETP* **67**, 2177 (1988).

[2] S. Schnetzer et al., *Phys. Rev.* **C 40**, 640 (1989); A. Shor et al., *Nucl. Phys.* **A 514**, 717 (1990); W. Cassing et al., *Phys. Lett.* **B 238**, 25 (1990); H. Müller, K. Sistemich, *Z. Phys.* **A 344**, 197 (1992); A.A. Sibirtsev, M. Büscher, *Z. Phys.* **A 347**, 191 (1994); W. Cassing et al., *Z. Phys.* **A 349**, 77 (1994); A.A. Sibirtsev, *Phys. Lett.* **B 359**, 29 (1995); M. Büscher et al., *Z. Phys.* **A 355**, 93 (1996); M. Debowski et al., *Z. Phys.* **A 356**, 313 (1996); A.A. Sibirtsev et al., *Z. Phys.* **A 358**, 357 (1997); A. Badala et al., *Phys. Rev. Lett.* **80**, 4863 (1998); Yu.T. Kiselev et al., *J. Phys.* **B 25**, 381 (1999).

[3] E.Ya. Paryev, *Eur. Phys. J.* **A 5**, 307 (1999).

[4] M. Büscher et al., *Z. Phys.* **A 351**, 333 (1995).

[5] W. Borgs et al., *COSY Proposal no. 18* (1991), unpublished.

[6] M. Büscher, Ph.D. Thesis, Universität zu Köln (1992).

[7] M. Büscher et al., *Proc. Int. Conf. on Mesons and Nuclei at Intermediate Energies*, Dubna, Russia, May 3–7, 1994, World Scientific Publishing, editors M.K.Khankhasayev and Z.B.Kurmanov, ISBN 981-02-1787-0, p.446 (1994).

[8] O.W.B. Schult et al., *Nucl. Phys.* **A 583**, 629 (1995).

[9] S. Barsov et al., *Nucl. Instr. Meth.* **A 462/3**, 364 (2001).

[10] S. Barsov et al., *Proc. 16th Int. Conf. on Magnetic Technology*, Sept. 26 – Oct. 2, 1999, Ponte Vedra Beach, USA, *Trans. Appl. Superconductivity* **10**, 1 (2000); H.J. Stein et al., *Rev. Scient. Instr.* in print.

[11] H. Müller, *Z. Phys.* **A 339**, 409 (1991).

[12] R. Schleichert, Ph.D. Thesis, Technische Hochschule Aachen (1996).

[13] L. von Horn, Ph.D. Thesis, Universität zu Köln (1996).

[14] H. Junghans, Ph.D. Thesis, Universität zu Köln (1999).

[15] M. French et al., *Nucl. Instr. and Meth.* **A 343**, 222 (1994).

[16] W. Erven et al., *IEEE Trans. Nucl. Sci.* **45**, 852 (1998).

[17] A. Schneider, Ph.D. Thesis, Universität zu Köln (1998).

[18] A. Franzen, Ph.D. Thesis, Universität zu Köln (1996).

[19] V.V. Abaev et al., *J. Phys.* **G14** 903 (1988).

[20] J. Papp et al., *Phys. Rev. Lett.* **34** 601 (1975).